scientific reports

Check for updates

OPEN

Displacement-based seismic fragility assessment of a high-rise reinforced concrete building

Keshav Kumar Sharma[1], Ashhad Imam[2], Pramod Kumar[3] & Bamidele Charles Olaiya[4]✉

This study presents a displacement-based seismic fragility assessment of a high-rise reinforced cement concrete (RCC) building designed in compliance with Indian seismic codes. The selected structure, a G+19 ordinary moment-resisting frame (OMRF), is modelled in ETABS with realistic material properties, geometric irregularities, and design loads as per IS 875 and IS 1893 provisions. Seismic performance evaluation is conducted through Incremental Dynamic Analysis (IDA) using a suite of ground motion records from FEMA P695, scaled progressively to capture structural response from elastic behaviour to collapse. Peak Ground Acceleration (PGA) and spectral displacement serve as intensity measures, while inter-storey drift ratio is adopted as the primary damage parameter. Fragility curves are developed for key performance levels based on maximum allowable drift limits. The results reveal significant sensitivity of the high-rise frame to torsional irregularities, with drift concentration occurring predominantly in the mid-height storeys. Probabilistic fragility functions indicate that the probability of exceeding life safety limits increases sharply beyond a PGA of 0.25g. Comparison with previous studies confirms that displacement-based assessment provides a more accurate representation of seismic vulnerability than force-based methods, particularly for irregular high-rise configurations. The findings emphasize the necessity for enhanced design considerations, including stiffness regularity and supplemental damping systems, to improve resilience in Indian high-rise RCC buildings. This research contributes a performance-based seismic assessment framework adaptable for both new designs and retrofitting strategies in similar structural systems.

Keywords Displacement-based design, Incremental dynamic Analysis, Fragility curves, Seismic performance, ETABS

The increasing frequency and intensity of seismic events have underscored the critical need to assess the vulnerability of structures, particularly high-rise reinforced concrete (RC) buildings. In this context, fragility analysis has become a vital component of earthquake engineering. It provides a probabilistic framework to evaluate the likelihood that a structure will experience different levels of damage when subjected to seismic excitation. Central to this methodology are fragility curves, which represent the probability of exceeding specific damage states as a function of seismic intensity measures, such as Peak Ground Acceleration (PGA) and Spectral Acceleration (Sa). These curves act as essential tools in performance-based earthquake engineering, supporting decisions related to seismic retrofitting, emergency response planning, and the design of resilient infrastructure[1,2].

Historically, force-based design methods dominated seismic assessments. However, they often fell short in capturing the inelastic and nonlinear behaviour of structures during strong earthquakes. As a result, displacement-based design philosophies have emerged, placing greater emphasis on deformation demands rather than forces. This shift aligns more directly with observed structural damage, making it a more accurate approach. Foundational contributions by Priestley & Kowalsky[3] and Moehle[4] promoted this philosophy by identifying inter-storey drift and spectral displacement as key indicators of seismic performance. Building upon this, Sullivan et al.[5] developed a systematic and codified framework for its practical implementation. The

[1]Department of Civil Engineering, National Institute of Technology Jamshedpur, Jamshedpur, Jharkhand 831014, India. [2]Department of Civil Engineering, Sam Higginbottom University of Agriculture Technology and Sciences, Prayagraj 211007, Uttar Pradesh, India. [3]Department of Civil Engineering, Graphic Era (Deemed to be University), Dehradun 517102, Uttarakhand, India. [4]Department of Civil Engineering, School of Engineering and Applied Sciences (SEAS), Kampala International University, Western Campus, Ishaka, Uganda. ✉email: bmolaiya@kiu.ac.ug

study applies this displacement-based methodology to assess the seismic fragility of a 19-storey RC building designed according to Indian seismic codes. The building's response to earthquake loading is evaluated through Incremental Dynamic Analysis (IDA), a method that subjects the structure to progressively scaled ground motion records until failure6, 7. This approach enables the development of IDA curves, which detail how the structure behaves under increasing seismic intensity. By capturing nonlinear response characteristics, IDA provides critical input for constructing fragility functions[8,9], making it a powerful tool for evaluating seismic performance in modern engineering practice.

In recent years, the use of fragility curves has become an essential tool in evaluating the seismic vulnerability of structures, particularly reinforced concrete (RC) high-rise buildings. A widely accepted methodology for constructing these curves involves the integration of time history data sets from FEMA P695 with nonlinear dynamic simulations conducted in ETABS. These time history records are a series of ground motion inputs that simulate earthquake effects. Each ground motion is scaled incrementally to reflect increasing levels of seismic intensity[10]. The structural model is then analyzed under these varying levels until collapse or a predefined damage threshold is reached. This iterative process helps develop a statistical relationship between seismic intensity measures and corresponding damage states, forming the basis of fragility curves.

The resulting fragility curves enable the classification of structural performance into three primary levels: Immediate Occupancy (IO), Life Safety (LS), and Collapse Prevention (CP). These performance levels align with criteria proposed by Kircil & Polat[11], which allow engineers to evaluate and communicate risk in a meaningful and standardized way. This categorization is crucial for both design and retrofitting of high-rise buildings in seismic zones.

Two key intensity measures underpin the fragility curve methodology: Peak Ground Acceleration (PGA) and Spectral Acceleration (Sa) at the fundamental period of vibration, T. These measures are especially relevant for high-rise structures, which typically exhibit longer natural periods due to their height and flexibility. As such, long-period ground motions are more impactful on these buildings compared to low-rise structures.[12] emphasised the importance of incorporating both short-period (0.2s) and long-period (1.0s) Sa values in the fragility analysis of RC high-rises to properly capture their dynamic behaviour across a range of seismic scenarios.

In addition to ground motion intensity, the nonlinear behaviour of materials and geometric irregularities significantly influence a building's fragility. Research by Hosseinpour & Abdelnaby[13] highlighted the advantages of fibre-based modelling techniques in capturing the deterioration of concrete and reinforcement over time. This modelling provides a more accurate picture of damage evolution, especially in mid- to high-rise RC buildings where inelastic behaviour plays a dominant role during earthquakes.

As buildings become taller and more complex, the asymmetry in floor plans introduces torsional irregularities, which further affect seismic performance. Studies by Aziminejad & Moghadam[14] and Kumar et al.[15] have shown that near-field ground motions can produce significant torsional responses, causing early and concentrated damage in lateral load-resisting systems. Such phenomena underline the necessity of including plan and vertical irregularities in fragility assessments, particularly for modern urban structures with unconventional architectural designs.

In response to these vulnerabilities, structural control strategies have been explored to mitigate seismic fragility. Kumar et al.[16] reviewed various control mechanisms such as base isolators and energy dissipation devices, demonstrating their role in reducing damage potential. These strategies, both passive and active, enhance the resilience of high-rise structures against earthquake-induced deformations, such as inter-storey drifts and lateral sways. Their application is especially critical in seismically active countries like India, where the surge in high-rise RC construction demands robust and sustainable engineering solutions.

Advancements in computational modelling and machine learning have further enhanced the ability to predict structural responses under seismic loads[1]. Kumar et al.[17] conducted nonlinear time history analyses that incorporated material nonlinearity and evaluated the response of asymmetric buildings to real earthquake records. Their study found that soft storey configurations, often present in buildings with open ground floors, are particularly vulnerable to collapse, reinforcing the need for thorough fragility assessments in such cases.

Another critical component in fragility analysis is the treatment of uncertainty. As emphasized by Cem & Ellingwood[18,] uncertainties in seismic response can be divided into aleatory (random variability in nature) and epistemic (due to lack of knowledge). Both types must be considered to ensure realistic and dependable fragility curves. Ghosh & Chakraborty[2] advanced this aspect by applying Bayesian regression techniques, which allow for more nuanced and uncertainty-aware predictions compared to traditional statistical methods. Similarly, Shetty et al. (2004) demonstrated how such probabilistic approaches are effective in capturing brittle failure mechanisms, while 19–21 validated Bayesian-based methods for assessing the seismic vulnerability of asymmetric RC buildings, supporting their use in complex structural analysis.

The selection and scaling of ground motion records play a pivotal role in this methodology. Following FEMA P695 guidelines ensures that the chosen records cover a wide spectrum of frequency content, duration, and amplitude, thereby capturing the full range of potential seismic demands. In addition, directionality of ground motions must be accounted for, especially in tall buildings with eccentric mass or stiffness distribution. As shown by[22], the orientation of seismic loads can significantly alter damage patterns, making it a critical parameter in fragility modelling.

Despite extensive studies on seismic fragility of reinforced concrete buildings, most prior work has concentrated on symmetric and idealized models, often neglecting the influence of geometric and mass irregularities that are increasingly prevalent in modern high-rise structures. In the Indian context, research efforts have largely been restricted to force-based design evaluations, which inadequately capture nonlinear deformation and collapse mechanisms under strong earthquakes. Furthermore, many existing fragility assessments rely on a limited number of ground motion records or simplified modelling assumptions, thereby constraining their applicability for realistic high-rise configurations and local seismic conditions.

Scope of study

To address these limitations, this study contributes a displacement-based fragility assessment of a realistic G+19 RC high-rise building designed in compliance with Indian codes and incorporating both plan and vertical irregularities. Using Incremental Dynamic Analysis (IDA) with 44 ground motion records from FEMA P695, the study explicitly captures torsional effects, stiffness irregularities, and collapse mechanisms. It analyses the modelled structure regarding story displacement, calculates the IDR%, evaluates the hinge condition for ground motion data up to the collapsed PGA, produces IDA curves for ground movements up to the collapsed PGA, and depicts the Fragility curve with collapse as the damage threshold. Structures with a design PGA of 0.15 g often demonstrate diminished vulnerability at design-level intensities in contrast to those with a design PGA of 3.0 g. The IDAs are expected to continue functional until a failure occurs. This research predominantly utilizes 44 sets of Time History data from FEMA P695 to construct fragility curves. The study intends to perform a thorough analysis of a high-rise asymmetric RCC structure, assess time history data for ground motions, compute IDR%, examine hinges up to the collapsed PGA, generate IDR curves for ground motion data up to the collapsed PGA, and create fragility curves for the collapsed PGA. Utilizing the method for inter-storey calculations, we can construct the fragility curve by employing the mean and standard deviation to represent the failure points or collapse hinges, which are then used to delineate the fragility curves. The G+19 RCC structure is selected for the assessment of fragility curves concerning displacement. The fragility curve is developed utilising a damping ratio of 5% and 44 ground motion data points. The inter-storey drift ratio for the elevated PGA is initially calculated, and for each PGA resulting in collapse, the hinge condition is evaluated.

The study uses these IDR results to evaluate performance levels categorized as Immediate Occupancy (IO), Life Safety (LS), and Collapse Prevention (CP), as per established fragility evaluation criteria. A damping ratio of 5% is applied throughout the dynamic simulations. Using the calculated IDR values and the corresponding PGA at which collapse occurs, fragility curves are developed. These curves express the probability of collapse as a function of PGA, fitted using a lognormal distribution with parameters such as mean and standard deviation derived from the IDA data. The curves enable a probabilistic understanding of the structure's vulnerability and are useful in seismic risk assessment, performance-based design, and retrofitting decisions.

Methodology

Linear analysis

The linear analysis methodology in this study involves the modelling and analysis of a G+19 asymmetric RC structure using ETABS software. The building is designed with vertical, planar, and mass irregularities, and the floor plan changes at every fifth level. The analysis begins by creating a three-dimensional model, with the material properties and frame section details (columns, beams, slabs) assigned as per the specifications provided in the design tables.

The dead and live loads are applied based on IS 875 (Part 1 and 2), with wall loads assigned as distributed loads on beams and floor loads applied as uniform shell loads on slabs. The self-weight of the structure is included using a self-weight multiplier of 1.0. A rigid diaphragm is assumed at each floor level to simulate in-plane rigidity (Table 4). The mass source is defined, and response spectrum load cases (RSX, RSY, and RSZ) are created for seismic analysis.

The linear static analysis uses the Response Spectrum Method as per IS 1893 (Part 1): 2016. The base shear forces in both X and Y directions are calculated and verified against code-specified values to ensure accuracy. Appropriate load combinations, including dead, live, and seismic loads, are defined according to the IS 1893:2016 standards.

After running the linear analysis, primary structural responses such as base shear, displacements, and story drifts are extracted and assessed. This forms the foundational step before proceeding to nonlinear static and dynamic analyses. The purpose of this phase is to verify the adequacy of the structural design under code-specified seismic loads and to ensure compliance with Indian seismic design standards. This linear assessment also helps identify potential vulnerabilities and validate the structural configuration before introducing nonlinear behaviours in further stages of the research.

Nonlinear static analysis

The nonlinear static analysis of the G+19 asymmetric RCC structure was performed after completing the linear analysis using ETABS. Gravity loads were first assigned, and P-Delta geometric nonlinearity was activated to account for second-order effects. Hinges were applied to structural elements to capture inelastic behaviour: beams were assigned "Auto Hinge Type" with M3 rotational hinges at both ends, while columns were assigned hinges based on ASCE 41-17 with "P-M2-M3" degrees of freedom. These hinges simulate potential plastic deformations under increasing lateral load. The model was saved and evaluated to confirm the hinge assignments and structural response.

This procedure enables the identification of failure zones and progressive deformation patterns under static lateral loading. The nonlinear static (pushover) analysis helped understand the sequence of plastic hinge formations and their locations, providing essential insights into the structural capacity and potential collapse mechanisms under seismic loading scenarios.

Nonlinear dynamic analysis

The nonlinear dynamic analysis in this study was conducted using time history analysis to simulate the real-time seismic response of a G+19 asymmetric RC structure. This approach involved applying 44 pairs of earthquake ground motion records sourced from FEMA P695. These records were selected to represent a wide range of seismic intensities and soil conditions, and they were scaled incrementally until structural collapse occurred.

Compatibility between time history and response spectrum data was ensured using SeismoMatch software, which adjusted ground motion records to match the target spectrum.

The analysis incorporated P-Delta geometric nonlinearity and used the nonlinear direct integration method in ETABS. Nonlinear hinge properties were assigned to frame elements: auto-generated M3 hinges for beams and P-M2-M3 hinges (ASCE 41-17) for columns. These hinges capture inelastic behaviour, such as yielding and plastic deformations[23]. For each earthquake record, the structure was analyzed under increasing intensity until a collapse mechanism was identified through the formation of collapse hinges.

Inter-storey drift ratios (IDR%) (Eq. 1) were computed from the displacements of adjacent floors, serving as performance indicators. These were compared against predefined thresholds for Immediate Occupancy (IO), Life Safety (LS), and Collapse Prevention (CP). The resulting IDR values at different Peak Ground Accelerations (PGAs) were used to generate Incremental Dynamic Analysis (IDA) curves, which illustrate the structure's deformation behaviour under varying seismic intensities.

$$IDR, \% = \frac{Upperstoreydisplacement - Lowerstoreydisplacement}{Floortofloorheight} * 100 \quad (1)$$

In this study, performance levels are classified based on inter-storey drift ratio (IDR) thresholds following Kircil & Polat[11] and ASCE 41-17 criteria. The limits are explicitly defined as: Immediate Occupancy (IO: IDR ≤ 0.5%), Life Safety (LS: 0.5% < IDR ≤ 0.8%), and Collapse Prevention (CP: IDR > 0.8%). From the Incremental Dynamic Analysis (IDA) results, these thresholds correspond approximately to PGA ≤ 0.24 g for IO, PGA ≈ 0.30–0.42 g for LS, and PGA ≥ 0.54 g for CP. These values were adopted to construct fragility curves and assess the seismic vulnerability of the studied structure.

For each ground motion set, the PGA at which the collapse hinge formed was recorded. These collapse points were statistically analyzed to derive the mean and standard deviation of the logarithmic PGA values. Using this data, fragility curves were constructed to express the probability of structural collapse as a function of PGA. This probabilistic representation enhances the understanding of seismic vulnerability and supports performance-based design, risk mitigation, and retrofitting strategies for high-rise RCC buildings in seismically active zones.

To ensure robustness of the modeling framework, a representative subset of nonlinear time history analyses was also repeated in the open-source platform SeismoStruct[24]. The inter-storey drift ratios and collapse PGA levels obtained were in close agreement with those from ETABS, with differences generally within 5–10%. This cross-validation confirms that the displacement-based fragility assessment framework is not limited to a single commercial tool and can be reliably reproduced using open-source modeling environments.

Building modelling

Ground motion selection and spectrum compatibility

The building model considered in this study is a G+19 reinforced cement concrete (RCC) high-rise structure exhibiting both plan and vertical irregularities to reflect realistic seismic design challenges. The total structural height is 60.6 m, with a uniform storey height of 3.0 m, and a plinth level elevated 0.6 m above the ground. The design intentionally incorporates plan modifications at every fifth storey to induce torsional effects and to capture the influence of mass and stiffness irregularities on seismic performance. Figs. 1, 2, 3, 4, 5, 6 and 7 illustrate the structural configuration, including the grid layout (Fig. 1), three-dimensional perspective (Fig. 2), and plan views of the ground floor (Fig. 3), lower storeys (Figs. 4 and 5), middle storeys (Fig. 6), and upper storeys (Fig. 7).

The nonlinear dynamic analysis in this study employed 44 ground motion records obtained from FEMA P695, representing a broad range of magnitudes, source-to-site distances, and frequency content. Each record was scaled incrementally until collapse was observed in the structural model, ensuring that the entire spectrum of seismic demand was captured.

To maintain consistency with Indian seismic code requirements, spectrum compatibility was ensured between the selected records and the target design response spectrum for Zone III conditions. This was achieved using the SeismoMatch software, which adjusts the frequency content of raw ground motions to closely align with the target spectrum while preserving essential characteristics such as duration, phase, and peak values. The compatibility validation confirmed that scaled records retained realistic dynamic features, enabling reliable simulation of the building's response under seismic loading.

By combining ground motion selection, incremental scaling, and spectrum compatibility in a single unified process, the methodology provides a robust basis for conducting Incremental Dynamic Analysis (IDA) and developing fragility curves.

SeismoMatch is a crucial instrument utilised to assess the compatibility of ground motions with a target response spectrum, an essential component of seismic analysis and design. Compatibility is essential for accurately incorporating seismic needs into design codes or site-specific analyses. SeismoMatch processes unrefined ground motion records while simultaneously modifying their frequency content. The response spectra are subsequently adjusted to closely align with the goal spectrum. Modifications are implemented using a wavelet-based technique that preserves intrinsic properties, including natural duration, phase, and peak values. This technique is iteratively performed until the modified ground motion aligns with the tolerance level of the target spectrum, so rendering it a realistic and dependable input for dynamic analysis. This is especially advantageous for managing varied ground motions, since users can analyse many records in a single session, hence enhancing efficiency in generating a set of spectrum-compatible motions. SeismoMatch provides engineers with powerful tools for evaluating structural responses and creating secure, resilient structures. This software enhances the use of ground motions, whether derived from natural records, synthetic motions, or scaled events, and guarantees dependable seismic performance.

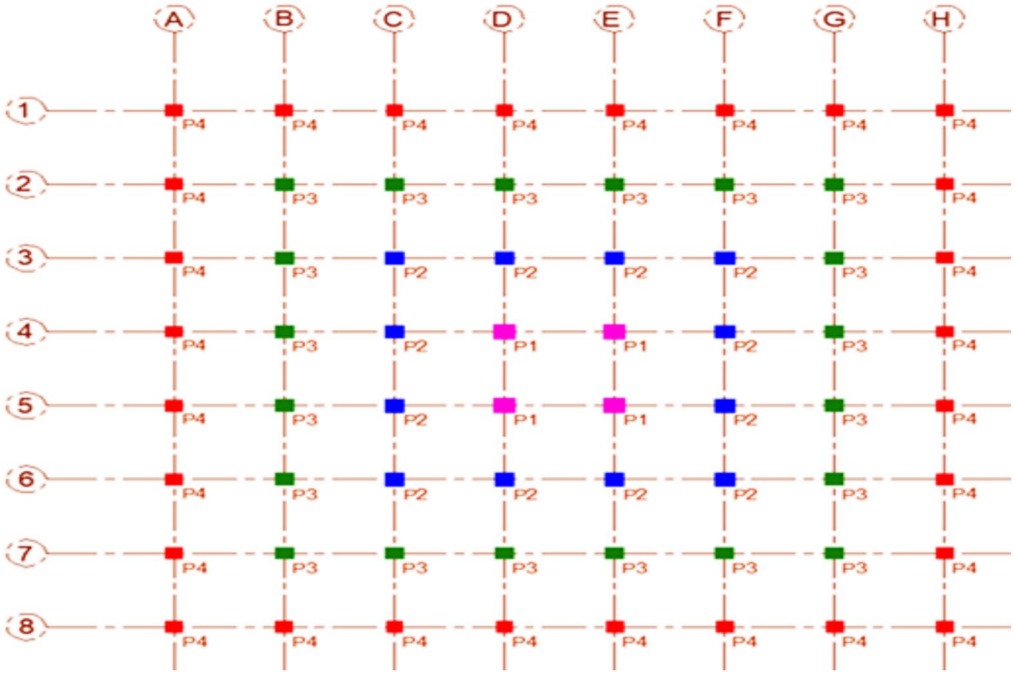

Fig. 1. Grid view of the building

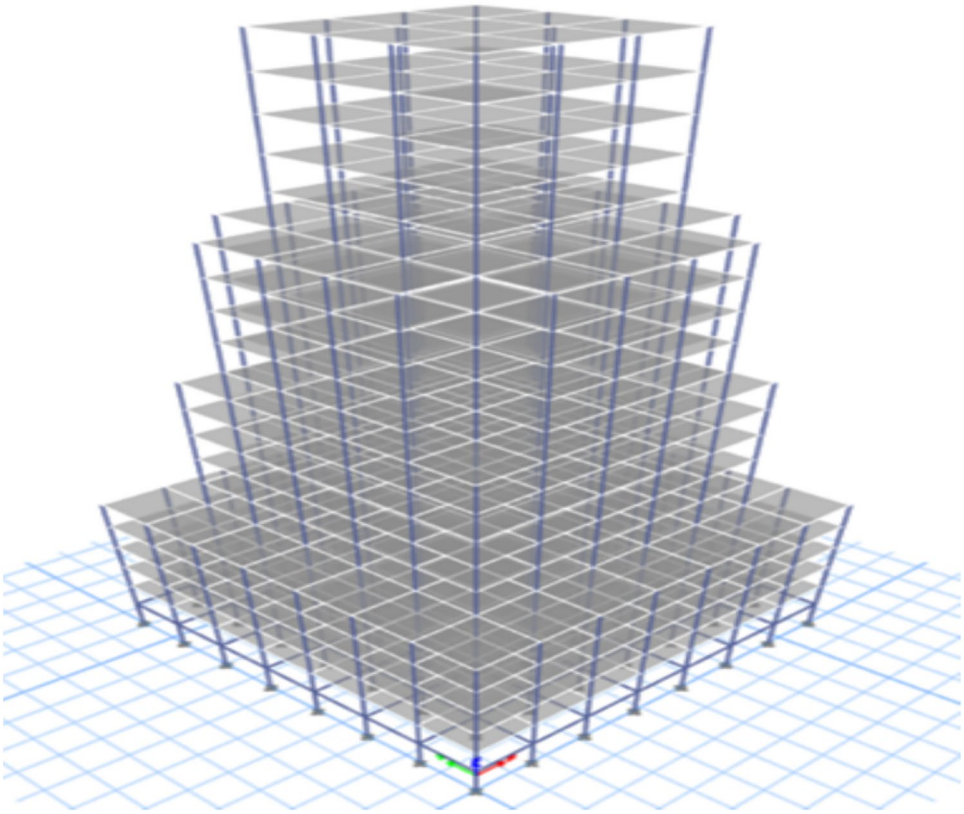

Fig. 2. 3-D View of building

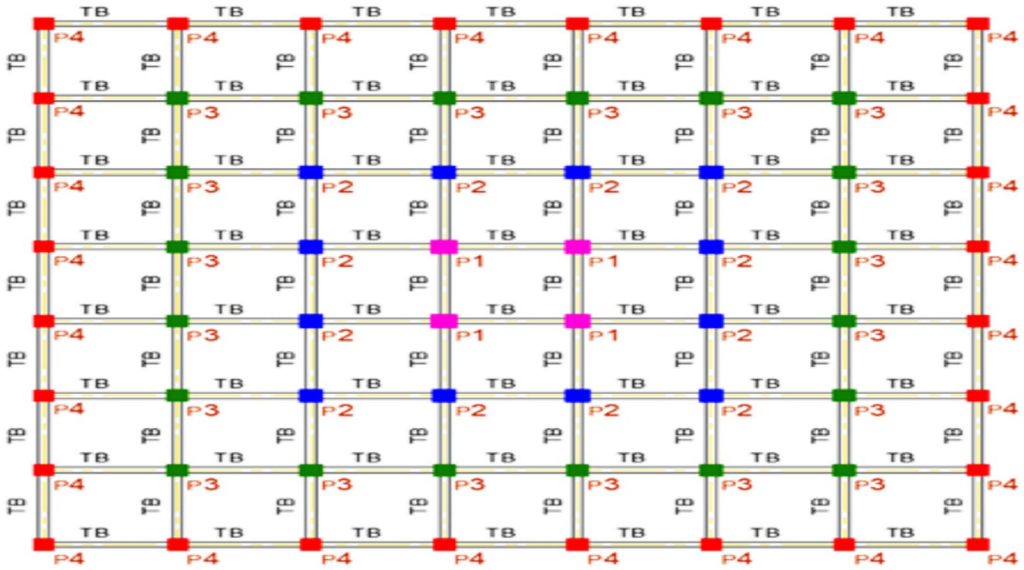

Fig. 3. Plan view of the ground floor

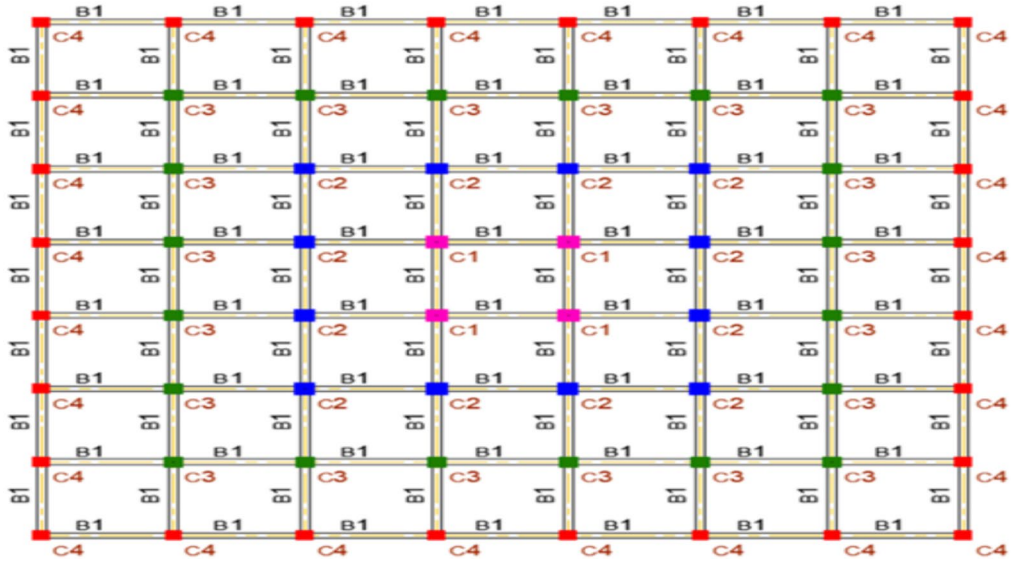

Fig. 4. Plan view of 1st to 4th floor

Material properties and sectional details

Material grades and sectional properties of the structural elements are defined to comply with Indian Standard (IS) codes. The columns, beams, and slabs are dimensioned based on storey level to optimize strength distribution and stiffness requirements (Table 1 and Table 2). For instance, foundation columns (P1–P4) range from 850 × 850 mm to 700 × 700 mm, while top-storey columns (C1c, C2c) are reduced to 400 × 400 mm to balance load demands with reduced axial forces. Beam depths vary between 450 mm and 500 mm, and slab thickness is maintained uniformly at 150 mm across all floors. The material parameters, including M30 grade concrete, Fe500 grade steel, unit weights, and elastic moduli, are summarized in Table 3.

Load considerations

All gravity and live loads are assigned according to IS 875 (Part 1 and Part 2) provisions. Dead loads include the self-weight of structural members, wall loads (external: 13.6 kN/m, internal: 7.4 kN/m, parapet: 2.5 kN/m), and floor finishes (1.0 kN/m^2 for typical floors, 2.4 kN/m^2 for the terrace). Live loads of 3.0 kN/m^2 are uniformly distributed on typical floors, while terrace floors have reduced live loading per code specifications (Table 4). The seismic parameters adopted in this study, summarized in Table 5, were defined in accordance with IS 1893 (Part 1): 2016. These parameters form the basis for the response spectrum analysis and ensure consistency with the seismic design requirements of Zone III conditions.

Fig. 5. Plan view of 5th to 9th floor

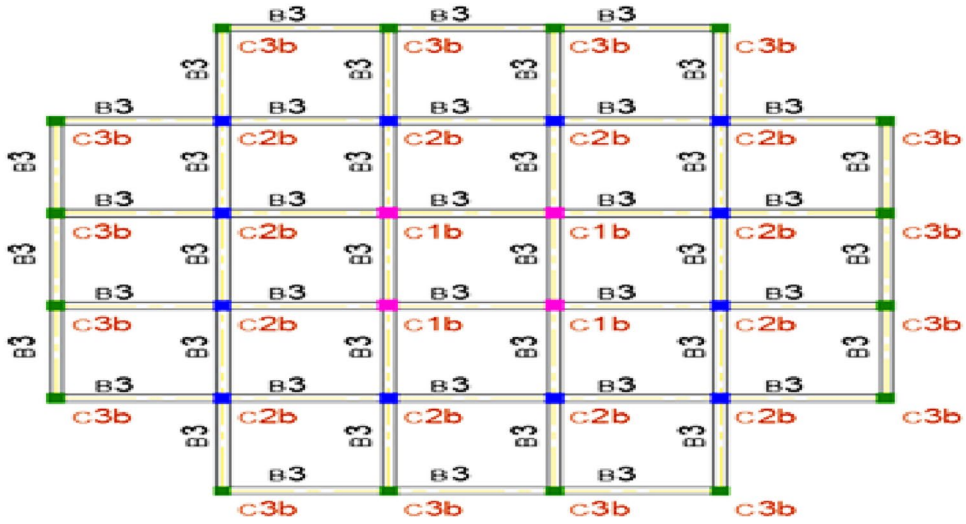

Fig. 6. Plan view of 10th to 14th floor

Modelling approach in ETABS

The structural model is developed in ETABS with careful definition of all material, section, and loading properties. A rigid diaphragm constraint is assigned at each floor to simulate in-plane stiffness of slabs, ensuring accurate distribution of lateral loads. The mass source includes dead loads and appropriate percentages of live loads to represent seismic mass. Response spectrum load cases (RSX, RSY, RSZ) are generated using the target design spectrum for Zone III.

Boundary conditions are fixed at the base to represent a fully restrained foundation, and static supports are applied in the vertical direction. The self-weight multiplier is set to 1.0 to ensure accurate gravity load simulation.

Results and discussions

The nonlinear dynamic analysis was carried out using 44 ground motion records, corresponding to 22 pairs of horizontal components (two orthogonal horizontal components each, resulting in a total of 44 ground motion records) obtained from the FEMA P695 database. These are presented in Table 6 as 22 earthquake events with their recording stations, where each event contributes two orthogonal horizontal components, making a total of 44 records. The hinge state, IDA versus PGA graph, and inter-storey drift ratio (IDR) data can be analyzed using these ground motions. Ultimately, we formulate fragility curves for the analyzed reinforced concrete frame construction. The structural collapse transpires at the spectral acceleration juncture when the curves diverge

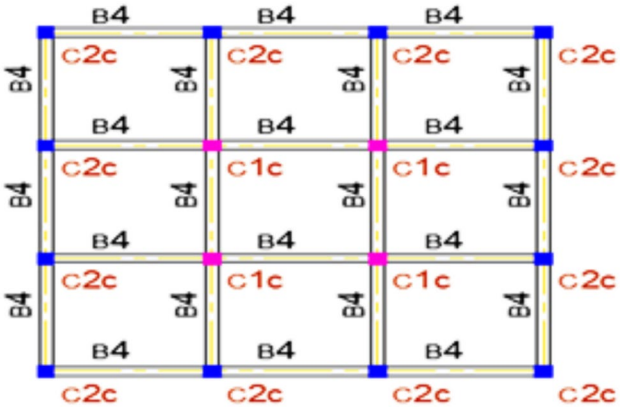

Fig. 7. Plan view of 15th to 19th floor

Floor Level		Inner Core	Outer Core	Mesosphere	Crust
16th to 19th	Name	C1c	C2c	—	—
	Dimension	400 mm × 400 mm	400 mm × 400 mm		
11th to 15th	Name	C1b	C2b	C3b	—
	Dimension	450 mm × 450 mm	400 mm × 400 mm	400 mm × 400 mm	
6th to 10th	Name	C1a	C2a	C3a	—
	Dimension	550 mm × 500 mm	500 mm × 500 mm	450 mm × 450 mm	
G to 5th floor	Name	C1	C2	C3	C4
	Dimension	650 mm × 650 mm	600 mm × 600 mm	550 mm × 500 mm	500 mm × 500 mm
Foundation to G	Name	P1	P2	P3	P4
	Dimension	850 mm × 850 mm	800 mm × 800 mm	750 mm × 750 mm	700 mm × 700 mm

Table 1. Sectional details of the column

Floor level	Name	Beam	Slab
G	TB	300 mm × 450 mm	150 mm
1st to 5th	B1	300 mm × 500 mm	150 mm
6th to 10th	B2	300 mm × 500 mm	150 mm
11th to 15th	B3	300 mm × 450 mm	150 mm
16th to 20th	B4	250 mm × 450 mm	150 mm

Table 2. Sectional details of beam and slab

Building parameters		Material parameters	
Structure	OMRF	Grade of concrete	M30
Number of stories	20	Grade of steel	Fe500
Plan area change	In every 5th story	Unit Weight of RCC	25 kN/m3
Height of the building	60.6 m	Unit Weight of Steel	7850 Kg/m3
Floor-to-floor height	3.0 m	Es	2 x 10^5 MPa
Soil type	Type II (Medium soil)	Ec	273 86.13 MPa

Table 3. Building and material parameters used in the study Es: Elastic modulus of steel; Es: Elastic modulus of concrete

from the linear path. Ground vibrations are amplified, and many non-linear dynamic analyses are performed until dynamic instability occurs.

The real-time information from simulated and/or actual earthquakes regarding ground acceleration is overlaid into the structural model over time. Subsequently, these data may be adjusted for the specific seismic

Type of Loads		Intensities	Type of Load Assigning	Code Used
Dead load	Wall load	13.6 kN/m (External walls)	Frame load (Distributed)	
		7.4 kN/m (Internal Walls)		
		2.5 kN/m (Parapet Walls)		
	Floor Load (Floor Finish)	1.0 kN/m2 (Typical floors)	Shell load (Uniform)	IS:875 (Part 1)-1987
		2.4 kN/m2 (Terrace floor)		
Live load	Floor Load	3 kN/m2 (Typical floors)	Shell load (Uniform)	IS:875 (Part 2)-1987

Table 4. Load type, intensity, and their assigning types

Seismic Parameters	Remarks
Seismic zones and zone factor	Zone III (Z = 0.16)
Importance factor	1.5
Response reduction parameter, R	5
Soil type	II
Damping ratio	5%

Table 5. Seismic parameters

	Earthquake			Recording Station
Earthquake ID	Magnitude	Year	Name	Name
12011	6.7	1994	Northridge	Beverly Hills - Mulhol
12012	6.7	1994	Northridge	Canyon Contury-WLC
12041	7.1	1999	Duzce, Turkey	Bolu
12052	7.1	1999	Hector Mine	Hector
12061	6.5	1979	Imperial Valley	Delta
12062	6.5	1979	Imperial Valley	El Centro Array #11
12071	6.9	1995	Kobe, Japan	Nishi-Akashi
12072	6.9	1995	Kobe, Japan	Shin-Osaka
12081	7.5	1999	Kocaeli, Turkey	Duzce
12082	7.5	1999	Kocaeli, Turkey	Arcelik
12091	7.3	1992	Landers	Yermo Fire Station
12092	7.3	1992	Landers	Coolwater
12101	6.9	1989	Loma Prieta	Capitola
12102	6.9	1989	Loma Prieta	Gilroy Array #3
12111	7.4	1990	Manjil, Iran	Abbar
12121	6.5	1987	Superstition Hills	El Centro Imp. Co.
12122	6.5	1987	Superstition Hills	Poe Road (temp)
12132	7	1992	Cape Mendocino	Rio Dell Overpass
12141	7.6	1999	Chi-Chi, Taiwan	CHY101
12142	7.6	1999	Chi-Chi, Taiwan	TCU045
12151	6.6	1971	San Fernando	LA - Hollywood Stor
12171	6.5	1976	Friuli, Italy	Tolmezzo

Table 6. Ground motion data considered according to FEMA P695

conditions that the structure will face. The structure will be modelled, and seismic data will be utilised to simulate ground shaking. Calculation of Peak Ground Acceleration (PGA) in this study was carried out by progressively scaling the acceleration time histories until the formation of a collapse hinge was detected in accordance with ASCE 41-17 criteria. At each intensity level, the inter-storey drift ratio (IDR) was evaluated using Eq. 1. The PGA corresponding to the intensity level that triggered global collapse was recorded for each of the 44 ground motion records. These collapsed PGAs were then statistically processed to compute the mean (λ) and standard

deviation (ζ) of the natural logarithm of PGA values. The collapse probability (P_f) was subsequently obtained using a lognormal cumulative distribution function (Eq. 2).

$$P_f\left(IM\right) = \phi\left(\frac{\ln\left(IM\right) - \lambda}{\zeta}\right) \tag{2}$$

Where IM represents the intensity measure (PGA) and ϕ is the standard normal cumulative distribution function.

Upon conducting this analysis for 44 ground motions, we obtain several collapse points from which we will compute the mean and standard deviation. The collapse potential is then derived from the formula utilising these statistical measures, followed by the construction of the fragility curve. This approach is based on the methodology established by Kircil and Polat[11] and the Baker[25] method for fragility function fitting through dynamic structural analysis. Engineers solve motion equations to analyse the temporal behaviour of structures. Results are analysed and compared to comprehend the structural response to various earthquake activity.

Realistic seismic analysis is facilitated by the congruence between the response spectrum and time history data. Figure 8 Spectrum. The compatibility between Response Spectrum and time history data demonstrates that the 44-ground motion can correspond with the anticipated seismic demand on a structure, thereby facilitating an accurate depiction of structural responses; it integrates consistency in design, site-specific characteristics, and detailed time-domain information not provided by response spectra. Spectrum compatibility guarantees regulatory compliance, validates models, facilitates iterative design optimization, and consequently fosters the development of safer and more reliable structures.

Ground motion selection and spectrum compatibility

In this study, 44 ground motion records were selected from the FEMA P695 database, which provides a standardized and widely accepted set of earthquake records for seismic performance assessment. These records span a magnitude range of 6.5–7.6 and include both near-field and far-field events (Table 6), thereby ensuring coverage of diverse fault mechanisms, frequency contents, and durations. Such diversity is essential for capturing the nonlinear seismic response of high-rise reinforced concrete buildings. The records were further processed using SeismoMatch software to achieve compatibility with the target response spectrum for Indian seismic Zone III conditions (Fig. 8). This ensured that the selected motions not only preserved key dynamic characteristics (e.g., amplitude, frequency content, and duration) but also realistically represented the seismic hazard for the study region. The use of FEMA P695 records was preferred over region-specific datasets because of their:

i. Widespread application in fragility and collapse assessments, enabling comparability with existing literature,
ii. Broad coverage of seismic scenarios relevant for probabilistic analyses, and

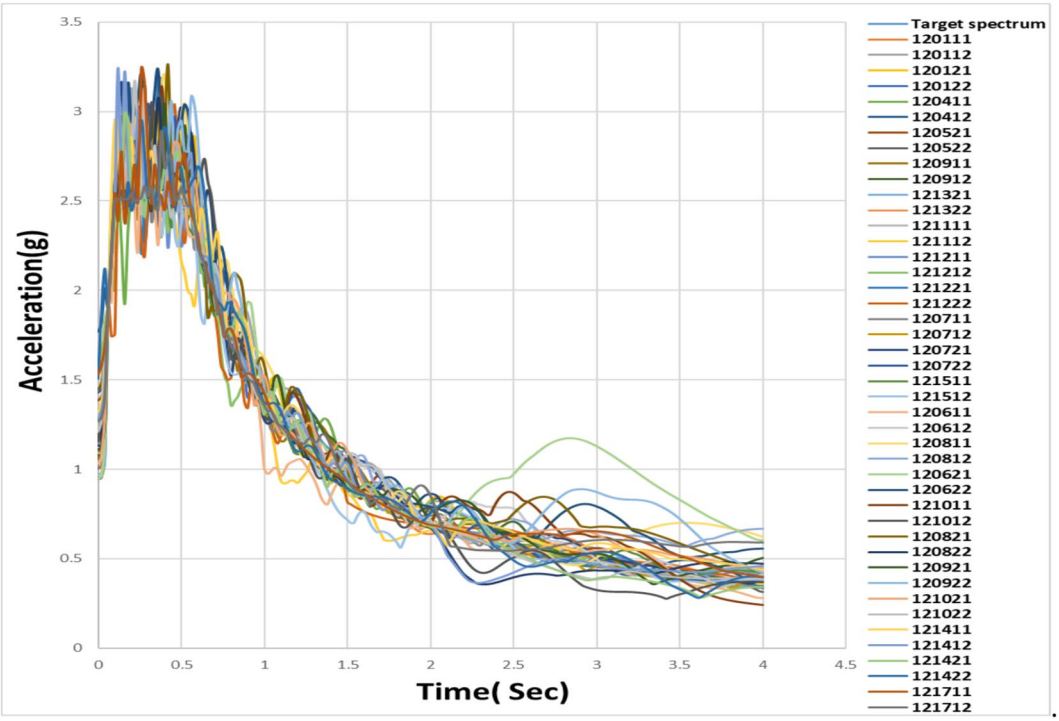

Fig. 8. Spectrum Compatible between the Response Spectrum and the time history data

iii. Inclusion of long-period components, which are particularly critical for evaluating the seismic vulnerability of tall buildings such as the G+19 RCC frame considered here.

It is important to note that some earthquake IDs, such as 120111 and 120112 (and similarly 120121/120122, 120911/120912, etc.), correspond to the same seismic event but were recorded at different stations. For example, as listed in Table 6, ID 120111 represents the Northridge (1994) record at Beverly Hills–Mulhol, whereas 120112 corresponds to the same event captured at Canyon Country–WLC. The differences observed between these spectra are therefore attributable to site-specific factors such as local soil conditions, station location relative to the epicenter, and variations in wave propagation paths. Including both records in the analysis is intentional, as it allows the fragility assessment to reflect realistic variability in structural demand arising from ground motion characteristics at different recording stations during the same earthquake.

Inter-storey drift ratio (IDR) response

For each ground motion set, the PGA was incrementally increased until the formation of collapse hinges, as defined by ASCE 41-17 criteria. The computed IDR values (Table 7) demonstrated a clear positive correlation with PGA. At lower intensity levels (PGA ≤ 0.24 g), IDR values generally remained below 0.5%, corresponding to the Immediate Occupancy (IO) performance level. Between PGA values of 0.30–0.42 g, most records produced IDRs in the 0.6–0.8% range, approaching or exceeding the Life Safety (LS) threshold. Collapse Prevention (CP) limits were typically reached beyond PGA ≈ 0.54 g, with IDRs surpassing 0.8% and, in some cases, exceeding 1.0%.

The variation in IDR response between ground motions at similar PGA levels can be attributed to differences in frequency content and duration, as well as the building's asymmetric configuration. Earthquakes with strong long-period components, such as the Chi-Chi and Kobe records, induced larger drifts due to resonance effects at the building's fundamental period.

It is acknowledged that PGA and spectral acceleration at the fundamental period Sa(T1) may not fully represent the seismic demand of high-rise buildings, where higher modes of vibration contribute significantly to the overall response. In this study, while PGA and Sa(T1) were employed as intensity measures for fragility curve development in line with FEMA P695 and prior literature, the actual structural performance evaluation was conducted using displacement-based parameters such as IDR and spectral displacement. These measures inherently capture the influence of higher modes and torsional irregularities through nonlinear time history analyses, ensuring that the dynamic effects characteristic of tall buildings are appropriately reflected in the fragility assessment.

It is noteworthy that the maximum inter-storey drift demands and hinge concentrations are observed near the 5th, 10th, and 15th storeys. These levels correspond directly to the locations of vertical irregularities introduced through plan area changes and column size transitions. This confirms that vertical irregularities significantly influence the seismic response by localizing deformation demands and accelerating the onset of nonlinear behaviour.

Table 7 presents the IDR values corresponding to different PGA levels for each ground motion record. In some cases, values are not reported at higher PGA levels because structural collapse occurred earlier, and further increments of PGA were therefore not applicable.

Incremental dynamic analysis (IDA) curves

The IDA curves (Fig. 9) provided a visual representation of the structure's nonlinear deformation behaviour across all seismic intensities. Initially, the curves displayed a near-linear relationship between PGA and IDR, indicating elastic response[26]. Beyond a PGA of approximately 0.36 g, many records exhibited curve softening, signaling the onset of significant inelastic deformations and hinge formation. The ultimate collapse points, marked by instability or global mechanism formation, varied from 0.24 g (most vulnerable records, e.g., Northridge Canyon) to 0.72 g (most robust records, e.g., Superstition Hills).

This range highlights the pronounced influence of ground motion characteristics on collapse capacity, even for the same structural configuration. The dispersion observed in collapse PGAs underscores the necessity of a probabilistic fragility approach rather than reliance on a single deterministic threshold.

Collapse mechanisms and hinge distribution

The nonlinear analysis revealed that plastic hinges predominantly formed at beam ends in the lower stories and at column bases in the podium and first five floors, as indicated by the red dots in Figure 10. This pattern is consistent with the concentration of seismic demand in stiffness transition zones[27, 28]. The asymmetric plan geometry introduced torsional effects that accelerated hinge formation on the stiffer side of the building, a finding aligned with previous studies on irregular structures[14]. At higher PGA levels (>0.54 g), hinge formation propagated rapidly through the vertical load-resisting system, culminating in collapse mechanisms involving combined flexural and shear failures.

Fragility curve development

Using the collapse PGA values from all 44 records, the mean logarithmic PGA (λ) was calculated as 0.4314, with a standard deviation (ζ) of 0.10621. A lognormal cumulative distribution function was fitted to the data to produce the fragility curve (Fig. 11). This curve quantifies the probability of collapse as a function of PGA and serves as a direct input for seismic risk assessment[29].

Using the collapse PGA values from all 44 records, the mean logarithmic PGA (λ) was calculated as 0.4314, with a standard deviation (ζ) of 0.10621. A lognormal cumulative distribution function was fitted to the data to produce the fragility curve (Fig. 11). This curve quantifies the probability of collapse as a function of PGA and

EQ ID	PGA vs IDR% VALUES								
120111	PGA	0.00	0.16	0.24	0.36	0.48	0.52	0.56	0.60
	IDR	0	0.2801	0.4194	0.6342	0.6699	0.7155	0.751	0.7765
120112	PGA	0.00	0.16	0.24	0.27	0.30	0.36	-	-
	IDR	0	0.3423	0.5183	0.5933	0.6746	0.8387	-	-
120121	PGA	0.00	0.16	0.24	0.30	0.33	0.36	-	-
	IDR	0	0.3292	0.4956	0.6211	0.6766	0.7241	-	-
120122	PGA	0.00	0.16	0.24	0.30	0.33	0.36	-	-
	IDR	0	0.3081	0.4632	0.5784	0.6375	0.6898	-	-
120411	PGA	0.00	0.16	0.24	0.36	0.42	0.45	0.48	-
	IDR	0	0.3227	0.4583	0.5841	0.649	0.6947	0.7552	-
120412	PGA	0.00	0.16	0.24	0.36	0.48	0.54	0.60	-
	IDR	0	0.2066	0.3099	0.465	0.6132	0.6737	0.7373	-
120521	PGA	0.00	0.16	0.24	0.36	0.48	0.60	0.66	-
	IDR	0	0.2125	0.3187	0.4793	0.63	0.7052	0.7694	-
120522	PGA	0.00	0.16	0.24	0.36	0.48	0.51	0.54	0.60
	IDR	0	0.2471	0.3706	0.5436	0.6903	0.7249	0.7249	0.7815
120911	PGA	0.00	0.16	0.24	0.27	0.30	0.36	-	-
	IDR	0	0.3438	0.5195	0.5947	0.6766	0.8349	-	-
120912	PGA	0.00	0.16	0.24	0.27	0.30	0.36	-	-
	IDR	0	0.3403	0.5145	0.5871	0.6596	0.7947	-	-
121321	PGA	0.00	0.16	0.24	0.27	0.30	0.36	-	-
	IDR	0	0.3996	0.6203	0.7099	0.7908	0.9528	-	-
121322	PGA	0.00	0.16	0.24	0.36	0.42	0.45	0.48	-
	IDR	0	0.2340	0.3511	0.5339	0.6339	0.6764	0.711	-
121111	PGA	0.00	0.16	0.24	0.36	0.48	0.54	-	-
	IDR	0	0.2833	0.419967	0.5454	0.6514	0.689167	-	-
121112	PGA	0.00	0.16	0.24	0.36	0.42		-	-
	IDR	0	0.2944	0.4419	0.661433	0.754533		-	-
121211	PGA	0.00	0.16	0.24	0.36	0.42		-	-
	IDR	0	0.2767	0.4151	0.629733	0.7368		-	-
121212	PGA	0.00	0.16	0.24	0.42	0.48	0.54	-	-
	IDR	0	0.2871	0.4237	0.5702	0.630933	0.643633	-	-
121221	PGA	0.00	0.16	0.24	0.48	0.54	0.6	0.66	0.72
	IDR	0	0.1733	0.2599	0.513	0.565167	0.611	0.6559	0.7053
121222	PGA	0.00	0.16	0.24	0.42	0.48	0.54	0.6	-
	IDR	0	0.2707	0.4055	0.574167	0.602633	0.6337	0.6821	-
120711	PGA	0.00	0.16	0.24	0.36	0.42	0.45	0.48	-
	IDR	0	0.3069	0.4552	0.657967	0.743067	0.776067	0.804133	-
120712	PGA	0.00	0.16	0.24	0.36	0.42	-	-	-
	IDR	0	0.4147	0.517367	0.6118	0.921867	-	-	-
120721	PGA	0.00	0.16	0.21	0.24		-	-	-
	IDR	0	0.4689	0.626367	0.7132		-	-	-
120722	PGA	0.00	0.16	0.24	0.30	0.36	-	-	-
	IDR	0	0.3479	0.5245	0.638833	0.7061	-	-	-
121511	PGA	0.00	0.16	0.24	0.42	0.48	0.54	-	-
	IDR	0	0.2364	0.3546	0.634633	0.721567	0.7886	-	-
121512	PGA	0.00	0.16	0.24	0.36	0.42	-	-	-
	IDR	0	0.2639	0.3959	0.5709	0.6752	-	-	-
120611	PGA	0.00	0.16	0.24	0.36	0.42	-	-	-
	IDR	0	0.2804	0.420633	0.642567	0.736367	-	-	-
120612	PGA	0.00	0.16	0.24	0.36	0.42	-	-	-
	IDR	0	0.2694	0.404	0.634267	0.742267	-	-	-
120811	PGA	0.00	0.16	0.24	0.3	0.36	-	-	-
	IDR	0	0.3935667	0.6026	0.762833	0.8904	-	-	-
120812	PGA	0.00	0.16	0.24	0.3	0.36	-	-	-
	IDR	0	0.3757	0.5179	0.555467	0.6561	-	-	-

Continued

EQ ID	PGA vs IDR% VALUES								
120621	PGA	0.00	0.16	0.24	0.3	0.36	-	-	-
	IDR	0	0.3577	0.487167	0.6091	0.723167	-	-	-
120622	PGA	0.00	0.16	0.24	0.36	0.42	0.45	-	-
	IDR	0	0.2394	0.3567	0.548333	0.634633	0.6698	-	-
121011	PGA	0.00	0.16	0.24	0.36	0.42	-	-	-
	IDR	0	0.2776	0.416	0.6005	0.6802	-	-	-
121012	PGA	0.00	0.16	0.24	0.42	0.45	-	-	-
	IDR	0	0.23	0.3451	0.618967	0.669967	-	-	-
120821	PGA	0.00	0.16	0.24	0.3		-	-	-
	IDR	0	0.3683	0.5591	0.686167		-	-	-
120822	PGA	0.00	0.16	0.24	0.36	0.48	0.54	-	-
	IDR	0	0.2204	0.3306	0.490833	0.6555	0.730867	-	-
120921	PGA	0.00	0.16	0.24	0.3	0.36	-	-	-
	IDR	0	0.3248	0.4811	0.5985	0.714367	-	-	-
120922	PGA	0.00	0.16	0.24	0.3	0.36	-	-	-
	IDR	0	0.3527	0.5332	0.6761	0.8058	-	-	-
121021	PGA	0.00	0.16	0.24	0.3	0.36	-	-	-
	IDR	0	0.2837	0.4245	0.528733	0.649133	-	-	-
121022	PGA	0.00	0.16	0.24	0.3	0.36	0.42	-	-
	IDR	0	0.2934	0.438	0.5401	0.648033	0.725	-	-
121411	PGA	0.00	0.16	0.24	0.36	0.42	0.48	0.54	-
	IDR	0	0.2007	0.301	0.452467	0.534933	0.610267	0.678633	-
121412	PGA	0.00	0.16	0.24	0.3	0.36	-	-	-
	IDR	0	0.3117	0.4675	0.598033	0.739867	-	-	-
121421	PGA	0.00	0.16	0.24	0.3	0.36	-	-	-
	IDR	0	0.325	0.4898	0.6307	0.7665	-	-	-
121422	PGA	0.00	0.16	0.24	0.36	0.42	0.48	0.54	-
	IDR	0	0.2364	0.3546	0.538067	0.634633	0.721567	0.7886	-
121711	PGA	0.00	0.16	0.24	0.42	0.48	-	-	-
	IDR	0	0.2167	0.3251	0.576967	0.67	-	-	-
121712	PGA	0.00	0.16	0.24	0.42	0.48	-	-	-
	IDR	0	0.2399	0.3599	0.6461	0.726967	-	-	-

Table 7. IDR analysis for ground motions

serves as a direct input for seismic risk assessment[30]. As highlighted in Figure 11, for the design hazard level of Zone III (PGA = 0.16 g), the collapse probability is approximately 0.9%, which is well below the FEMA P695 acceptable threshold. However, at PGA = 0.36 g, the collapse probability rises to about 35%, and at PGA = 0.54 g, it exceeds 85%, clearly demonstrating the rapid escalation of collapse risk beyond the design level.

To further enhance clarity and demonstrate the statistical robustness of the findings, a summary of the key collapse PGA statistics, associated fragility probabilities, and corresponding IDR thresholds is presented in Table 8. This table provides a concise overview of the quantitative outcomes discussed above.

Conclusions

This study presented a displacement-based seismic fragility assessment of a high-rise reinforced concrete (RCC) G+19 building designed in accordance with Indian seismic codes. Using Incremental Dynamic Analysis (IDA) in ETABS, the building's seismic performance was evaluated under a suite of ground motion records from FEMA P695, considering inter-storey drift ratios and spectral displacement as the primary engineering demand parameters. Fragility curves were developed for different performance levels, enabling a probabilistic estimation of damage likelihood at varying seismic intensities.

The results indicate that the building exhibits progressive stiffness degradation and increasing drift demands with higher seismic excitation levels. The derived fragility curves clearly capture the transition from Immediate Occupancy to Life Safety and ultimately to Collapse Prevention states, with the probability of exceedance rising sharply beyond certain intensity thresholds. The influence of geometric irregularities was also reflected in localized drift concentration and early hinge formation, underscoring the importance of incorporating realistic plan and elevation variations in high-rise fragility studies.

The findings reinforce the suitability of displacement-based assessment frameworks for high-rise structures, as they provide a more direct correlation between structural response and expected damage than force-based approaches. Moreover, the probabilistic nature of fragility analysis offers a robust decision-making tool for performance-based seismic design and retrofit prioritization. The study also highlights that irregularities and

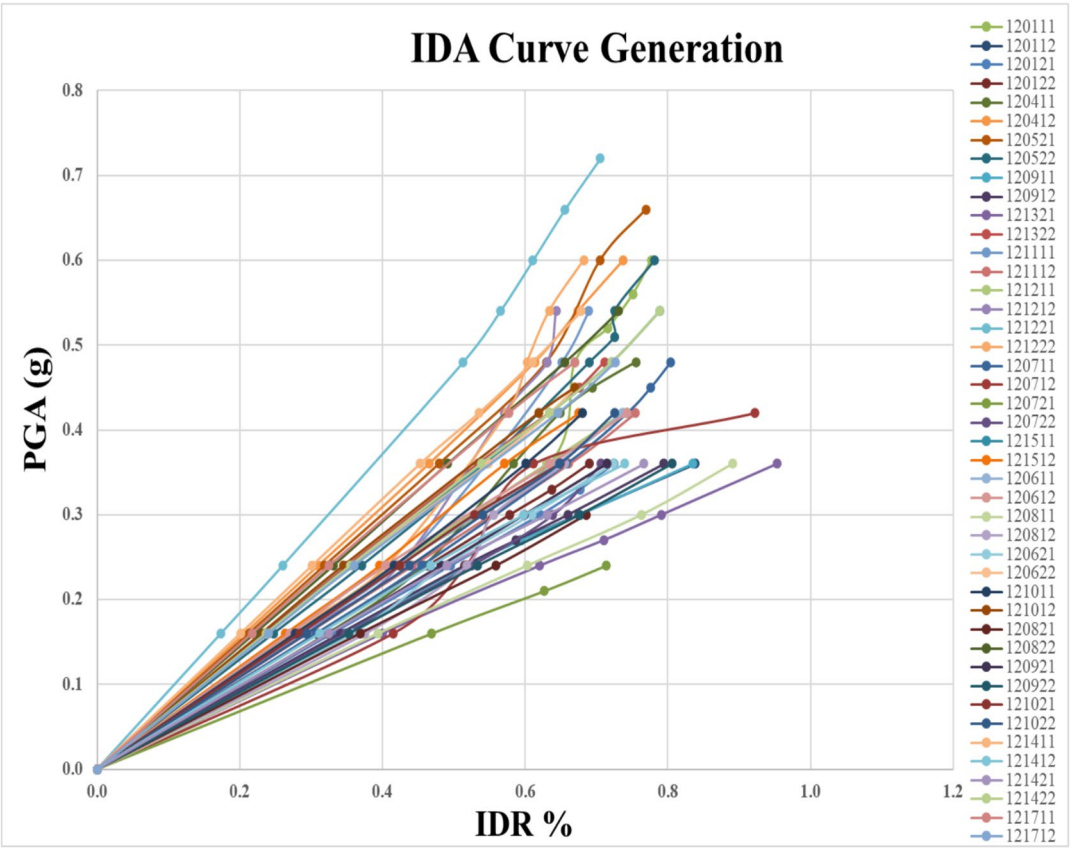

Fig. 9. IDA curve generation for the ground motions

material nonlinearity significantly influence collapse probabilities, necessitating their careful consideration in future code development and design practice.

Limitations and future scope

This study, while offering valuable insights into displacement-based seismic fragility assessment of a high-rise RCC building, is limited by idealized ETABS modelling with uniform material properties, fixed-base conditions, and no soil–structure interaction (SSI). Such simplifications overlook real-world factors like material variability, ageing, and soil flexibility. The fragility curves, based on a limited FEMA P695 ground motion set and only PGA/Sa intensity measures, may not fully represent the range of seismic hazards in Indian contexts, especially near-field pulse-type events. Non-structural elements were also excluded, despite their potential influence on stiffness, damping, and failure modes. Damage thresholds were adapted from literature and may require calibration to local data.

Future work could incorporate SSI, region-specific ground motions, and non-structural components for more realistic modelling. Broader intensity measures and advanced probabilistic techniques like Bayesian updating could improve accuracy. Extending analyses to retrofit strategies, comparing displacement- and energy-based approaches, and linking fragility to loss estimation would enhance the applicability of results to seismic risk mitigation and resilience planning.

Another limitation of this study is that the seismic fragility assessment was carried out solely in compliance with Indian seismic codes (IS 1893:2016, IS 875, and IS 456). Although this provides valuable insight within the national context, a broader comparison with international seismic design codes such as ASCE 7/41 (United States), Eurocode 8 (Europe), and JRA (Japan) could yield a more comprehensive understanding of global design philosophies and safety margins. Future research could extend the present framework to incorporate these international codes, thereby enabling cross-regional benchmarking of fragility outcomes and offering comparative insights into the relative conservatism or leniency of different seismic design provisions.

It is important to note that although OMRFs are not permitted for new construction in seismic Zones III, IV, and V under IS 1893 (2016), the present study does not advocate their use. The OMRF building considered here is chosen to represent existing building stock that was designed prior to the enforcement of current seismic provisions. The intention is solely to evaluate the seismic fragility of such structures and to provide insights that may guide retrofitting and risk mitigation strategies.

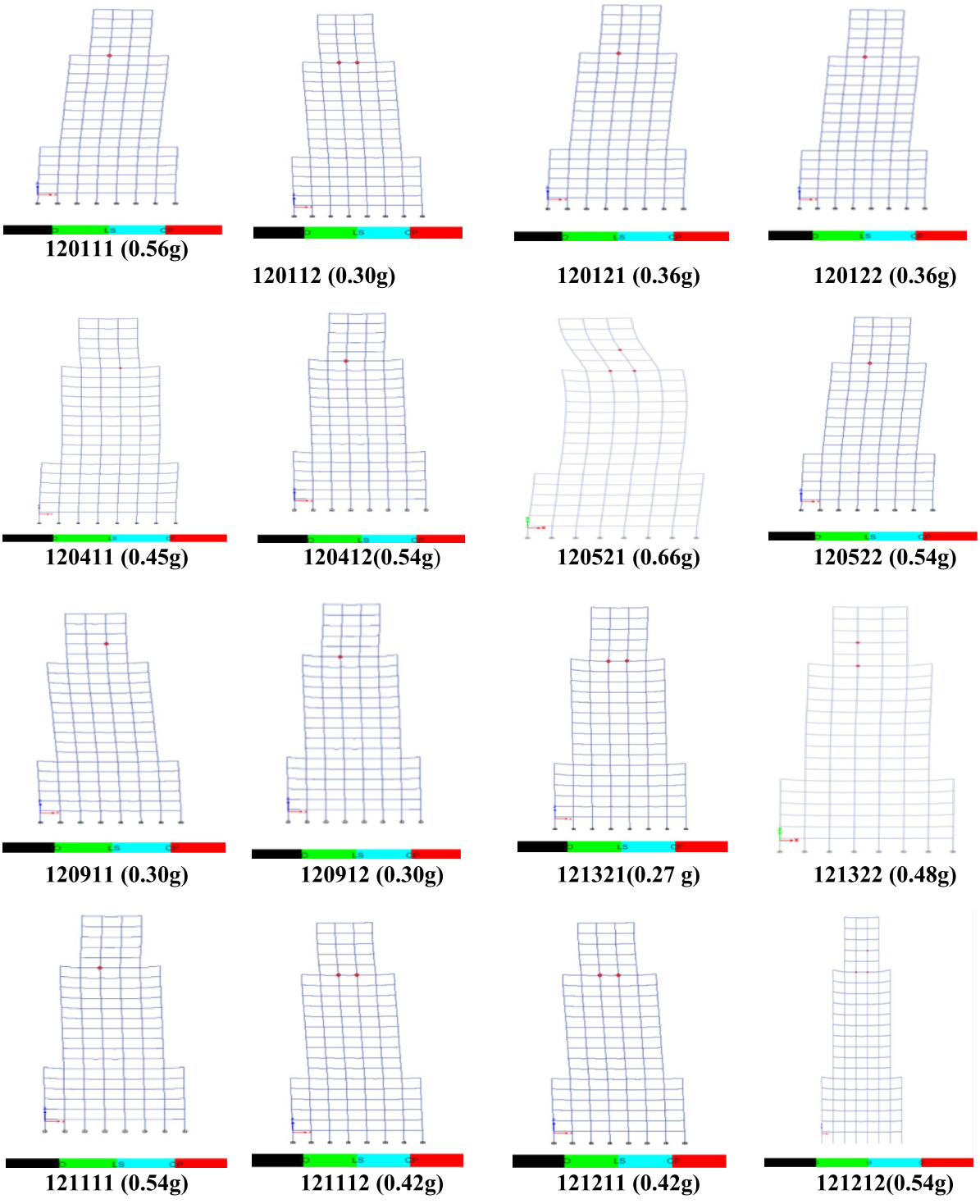

Fig. 10. Collapsed hinges formed for different earthquake sets

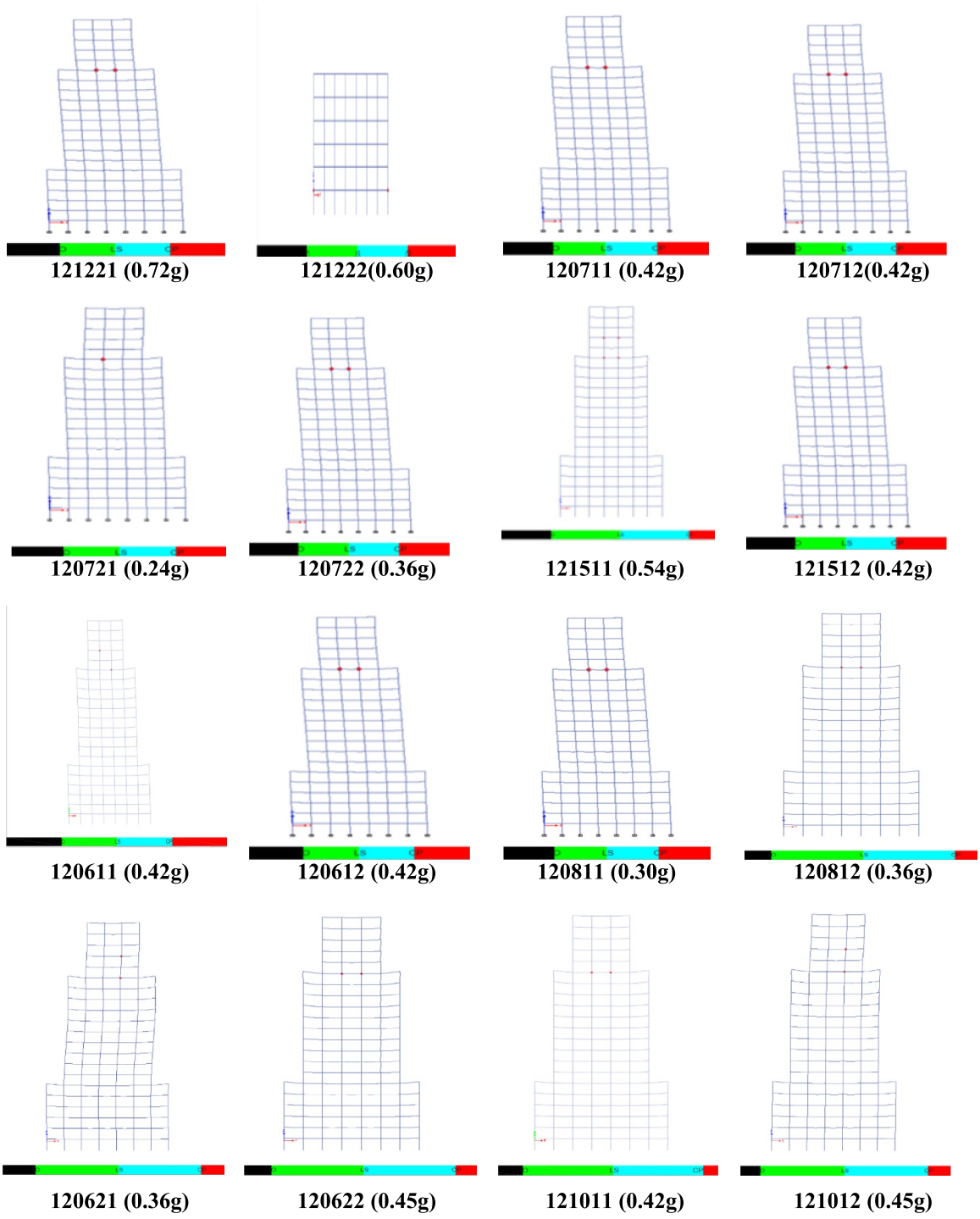

Fig. 10. (continued)

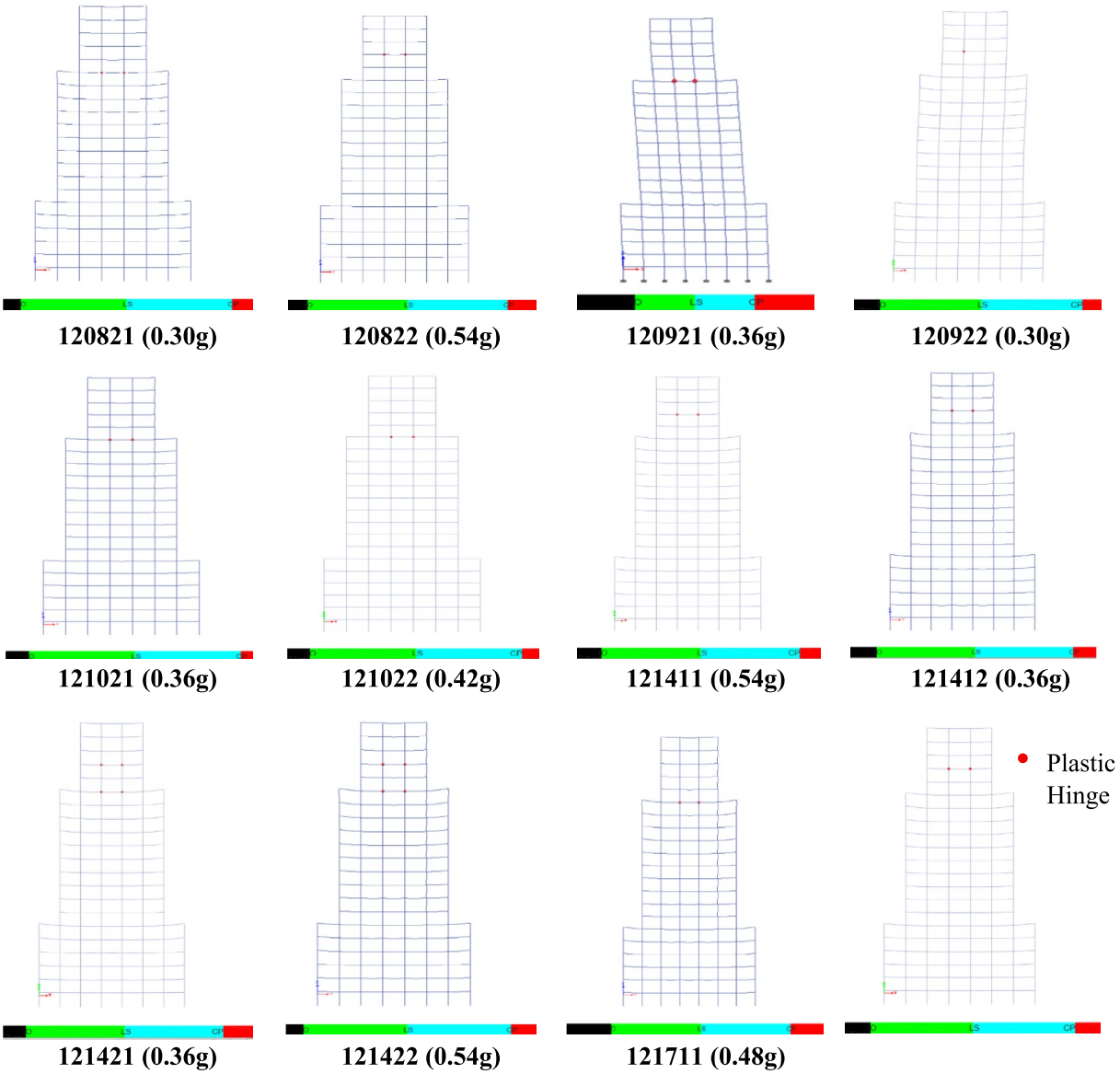

Fig. 10. (continued)

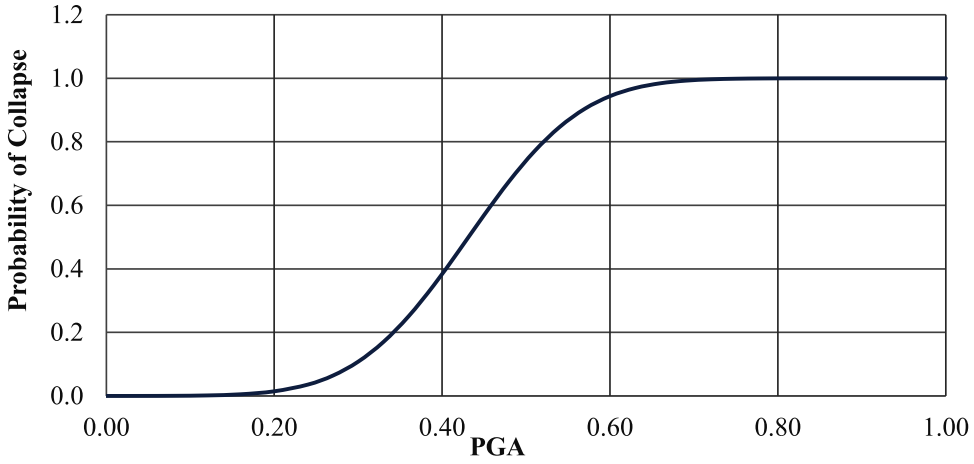

Fig. 11. Fragility curve for the G+19 RCC structure showing the probability of collapse as a function of PGA

Parameter / PGA Level	Value / Result	Interpretation
Number of ground motions	44	Total records used from FEMA P695
Mean logarithmic PGA (λ)	0.4314	Central tendency of collapse capacity
Logarithmic Std. deviation (ζ)	0.1062	Dispersion capturing variability
Minimum collapse PGA	0.24 g	Most vulnerable ground motion (Northridge Canyon)
Maximum collapse PGA	0.72 g	Most robust ground motion (Superstition Hills)
Collapse probability at 0.16 g	0.9%	Safe margin at the Zone III design level
Collapse probability at 0.36 g	35%	Significant risk at 2× design level
Collapse probability at 0.54 g	> 85%	Very high probability of collapse
Typical IDR at PGA ≤ 0.24 g	≤ 0.5%	Immediate Occupancy (IO)
Typical IDR at 0.30–0.42 g	0.6–0.8%	Life Safety (LS) threshold reached
Typical IDR at ≥ 0.54 g	≥ 0.8–1.0%	Collapse Prevention (CP) exceeded

Table 8. Statistical summary of collapse PGA values and fragility probabilities

Data availability

Data used in the study is present in the manuscript.

Received: 14 August 2025; Accepted: 26 September 2025
Published online: 03 November 2025

References

1. Jeong, S., Mwafy, A. M. & Elnashai, A. S. Probabilistic seismic performance assessment of code-compliant multi-story RC buildings. *Eng. Struct.* **34**, 527–537. https://doi.org/10.1016/j.engstruct.2011.10.019 (2012).
2. Ghosh, S. & Chakraborty, S. Seismic fragility analysis of structures based on Bayesian linear regression demand models. *Mech. Probab. Eng.* https://doi.org/10.1007/s11803-022-2082-7 (2020).
3. Priestley, M. J. N. & Kowalsky, M. J. Direct displacement-based seismic design of concrete buildings. *Bullet. New Zealand Soc. Earthq. Eng.* **33**(4), 421–444. https://doi.org/10.5459/bnzsee.33.4.421-444 (2000).
4. Moehle, J. P. Displacement-based design of RC structures subjected to earthquakes. *Earthq. Spectra* **8**(3), 403–428. https://doi.org/10.1193/1.1585688 (1992).
5. Sullivan, T. J., Priestley, M.J., & Calvi, G.M. A Model Code for the Displacement-based Seismic Design of Structures. *DBD12*, ISBN 9788861980723, IUSS Press, Pavia, 105pp. https://doi.org/10.1193/1.2932170 2012
6. Mishra, P., Srivastav, A., Kumar, P. & Sahu, S. K. Comprehensive review of seismic performance assessment for skew-reinforced concrete box-girder bridges. *Asian J. Civil Eng.* **25**(4), 3285–3299. https://doi.org/10.1007/s42107-023-00979-6 (2024).
7. Vamvatsikos, D. & Cornell, C. A. Incremental dynamic analysis. *Earthq. Eng. & Struct. Dyn.* **31**(3), 491–514. https://doi.org/10.1002/eqe.141 (2002).
8. Lagaros, N. D. Multicomponent incremental dynamic analysis considering variable incident angle. *Struct. Infrastruct. Eng.* **6**(1–2), 77–94. https://doi.org/10.1080/15732470802663805 (2009).
9. Lombardi, L. & De Luca, F. Derivation of fragility curves at design stage through linear time-history analysis. *Eng. Struct.* **219**, 110900. https://doi.org/10.1016/j.engstruct.2020.110900 (2020).
10. Kappos, A. J. & Manafpour, A. Seismic design of RC buildings with the aid of advanced analytical techniques. *Eng. Struct.* **23**(4), 319–332. https://doi.org/10.1016/S0141-0296(00)00052-3 (2001).
11. Kircil, M. & Polat, Z. Fragility analysis of mid-rise R/C frame buildings. *Eng. Struct.* **28**(9), 1335–1345. https://doi.org/10.1016/j.engstruct.2006.01.004 (2006).
12. Ji, J., Elnashai, A. S. & Kuchma, D. A. Seismic fragility relationships of reinforced concrete high-rise buildings. *Struct. Design Tall Spec. Build.* **18**(3), 259–277. https://doi.org/10.1002/tal.408 (2009).
13. Hosseinpour, F. & Abdelnaby, A. E. Fragility curves for RC frames under multiple earthquakes. *Soil Dyn. Earthq. Eng.* **98**, 222–234. https://doi.org/10.1016/j.soildyn.2017.04.013 (2017).
14. Aziminejad, A. & Moghadam, A. S. Fragility-based performance evaluation of asymmetric single-story buildings in near field and far field earthquakes. *J. Earthq. Eng.* **14**(6), 789–816. https://doi.org/10.1080/13632460902837728 (2010).
15. Kumar, P., Gogineni, A., Sahu, S. K., Singh, A. K. & Olaiya, B. C. A comprehensive review of response control systems for irregular buildings: exploring base isolators and dampers. *Discover Appl. Sci.* **7**(8), 809. https://doi.org/10.1007/s42452-025-07469-1 (2025).
16. Kumar, P., Madhuri, S. & Ahmed, M. Sequential nonlinear time history analysis of asymmetric reinforced concrete buildings under the 2011 great japan earthquake and tsunami. *Buildings* **15**(13), 2170. https://doi.org/10.3390/buildings15132170 (2025).
17. Kumar, P., Madhuri, S. & Olaiya, B. C. Nonlinear response analysis of plan and vertical asymmetric reinforced concrete buildings under directional seismic loadings. *Sci. Rep.* **15**(1), 27508. https://doi.org/10.1038/s41598-025-12737-6 (2025).
18. Cem, O. & Ellingwood, B. R. Seismic fragilities for non-ductile reinforced concrete frames –Role of aleatoric and epistemic uncertainties. *Struct. Saf.* **32**, 1–12. https://doi.org/10.1016/j.strusafe.2009.04.003 (2010).
19. Madhuri, S., & Kumar, P. Seismic analysis of vertical asymmetric RC Building. In symposium in earthquake engineering (pp. 219-231). Singapore: Springer Nature Singapore. https://doi.org/10.1007/978-981-99-1604-7_17 2022
20. Madhuri, S., & Kumar, P. Free vibration analysis of symmetric and asymmetric RCC structures. In IOP Conference Series: Materials Science and Engineering (Vol. 1273, No. 1, p. 012010). IOP Publishing. https://doi.org/10.1088/1757-899X/1273/1/012010 2023
21. Madhuri, S. & Kumar, P. Response of asymmetric reinforced concrete buildings under directional seismic loads. *Asian J. Civil Eng.* **25**(2), 1625–1640. https://doi.org/10.1007/s42107-023-00867-z (2024).
22. Vargas Alzate, Y. F. et al. Probabilistic seismic damage assessment of reinforced concrete buildings considering directionalityeffects. *Struct. Infrastruct. Eng.* **14**(6), 817–829. https://doi.org/10.1080/15732479.2017.1385089 (2017).
23. Bai, J., Yang, T. Y. & Ou, J. Improved performance based plastic design of RC moment resisting frames: Development and a comparative study. *Int. J. Struct. Stab. Dyn.* **18**(4), 1–24. https://doi.org/10.1142/S0219455418500505 (2018).
24. Seismosoft, 2022. SeismoStruct 2022 – A computer program for static and dynamic nonlinear analysis of framed structures. 2022
25. Baker, J. W. Efficient analytical fragility function fitting using dynamic structural analysis. *Earthq. Spectra* **31**(1), 579–599. https://doi.org/10.1193/021113EQS025M (2015).

26. Wen, T., Jiang, L., Jiang, L., Zhou, W. & Du, Y. Optimal intensity measure selection in incremental dynamic analysis: methodology improvements and application to a high-speed railway bridge. *Bullet. Earthq. Eng.* **22**(4), 2059–2083. https://doi.org/10.1007/s10518-023-01840-6 (2024).
27. Altiok, T. Y. Structural performance analysis of a retrofitted school building collapsed in Kahramanmaras earthquakes and evaluation of applied retrofitting methods. *Bullet. Earthqu. Eng.* https://doi.org/10.1007/s10518-025-02239-1 (2025).
28. Tan, K. H. Progressive collapse behaviour of advanced precast reinforced concrete joints with headed bars and plastic hinge relocation. *Eng. Struct.* **293**, 116603. https://doi.org/10.1016/j.engstruct.2023.116603 (2023).
29. Sandoli, A., Calderoni, B., Lignola, G. P. & Prota, A. Seismic vulnerability assessment of minor Italian urban centres: development of urban fragility curves. *Bullet. Earthq. Eng.* **20**(10), 5017–5046. https://doi.org/10.1007/s10518-022-01385-0 (2022).
30. Karimi Ghaleh Jough, F., & Ghasemzadeh, B. Uncertainty interval analysis of steel moment frame by development of 3D-Fragility curves towards optimized fuzzy method. Arabian Journal for Science and Engineering, 49(4), 4813-4830. https://doi.org/10.1007/s13369-023-08223-8 2024

Acknowledgements
The authors gratefully thank the authors' respective institutions for their strong support of this study.

Author contributions
The authors have significantly contributed to this article's development and writing. Keshav Kumar Sharma: Conceptualization, Data curation, Formal analysis, Investigation, Writing - original draft. Ashhad Imam: Project administration, Data curation, Formal analysis, Investigation, Writing – original draft, Writing – review and editing. Pramod Kumar: Writing – original draft, Writing – editing. Bamidele Charles Olaiya: Writing – original draft, Writing – review and editing.

Declarations

Competing interests
The authors declare no competing interests.

Ethical statement
This study did not involve human participants or animals; no ethical approval was required. All research procedures adhered to relevant ethical guidelines and best practices for non-human and non-animal research.

Declaration of AI use
The authors declare they will not use AI-assisted technologies to create this article.

Statement of originality
The authors declare that this manuscript is original, has not been published before and is not currently being considered for publication elsewhere. The authors confirm that the manuscript has been read and approved by all named authors and that no other persons have satisfied the criteria for authorship but are not listed. The authors further confirm that all have approved the order of authors listed in the manuscript of us. The authors understand that the corresponding author is the sole contact for the Editorial process. The corresponding author is responsible for communicating with the other authors about progress, submissions of revisions and final approval of proofs.

Additional information
Correspondence and requests for materials should be addressed to B.C.O.